since 1961

Baltica

BALTICA Volume 36 Number 1 June 2023: 63–78
https://doi.org/10.5200/baltica.2023.1.6

An evaluation of the characteristic aftershock parameters following the 24 January 2020 M_W = 6.8 Elazığ-Sivrice (Türkiye) earthquake

Serkan Öztürk

Öztürk, S. 2023. An evaluation of the characteristic aftershock parameters following the 24 January 2020 M_W = 6.8 Elazığ-Sivrice (Türkiye) earthquake. *Baltica, 36 (1)*, 63–78. Vilnius. ISSN 1648-858X.
Manuscript submitted 7 April 2023 / Accepted 4 May 2023 / Available online 19 June 2023

Abstract. A comprehensive evaluation of region-time-magnitude behaviours of aftershocks following the 24 January 2020 (*M*w = 6.8) Elazığ-Sivrice (Türkiye) earthquake was achieved by using the characteristic parameters such as *b*-value, *p*-value, *Dc*-value and Ma_{max} value of aftershock occurrences. The *b*-value was calculated as 0.82 ± 0.02 by considering the magnitude of the completeness value as *Mcomp* = 1.9, and it is relatively small compared to typical $b \approx 1$ for the magnitude-frequency relationship of aftershocks. This low *b*-value may also be caused by the abundance of aftershocks with $M_L \geq 4.0$. The *p*-value was computed as 0.80 ± 0.02 with *c*-value = 0.279 ± 0.098 and is smaller than the global value of $p \approx 1$. This low *p*-value may be due to a relatively slow decay rate of aftershock activity, and the modified Omori model seems appropriate for the estimation of decay parameters. The *Dc*-value was estimated as 1.87 ± 0.07. This large value shows that aftershocks are homogeneously distributed and more clustered at larger scales/in smaller areas. The temporal variation of *b*-value indicates that decreases in *b*-value may result from the gradual increase in the effective stress following the larger aftershocks. The lowest *b*-values and Ma_{max} values greater than 5.0 were observed in the north, south and southwest parts of the mainshock including Pütürge and Erkenek segments. These results show that there is an apparent relation between the smallest *b*-values and the largest Ma_{max} values. The largest *p*-values were estimated in and around the main shock including Pütürge segment. The regions with the smallest *b*-value and the largest *p*-value have high stress and coseismic deformation, respectively. Stress variations and coseismic deformation are extremely effective on the changes of *b*- and *p*-values. As a remarkable result, aftershock hazard following the mainshock may be considered extremely related to aftershock parameters, and detailed analyses of the region-time-magnitude characteristics of aftershocks are recommended for a preliminary evaluation following the mainshock.

Keywords: *aftershock hazard; Ma_{max} value; b-value; p-value; Dc-value*

Serkan Öztürk (serkanozturk@gumushane.edu.tr), http://orcid.org/ 0000-0003-1322-5164
Gümüşhane University, Department of Geophysics, TR-29100, Gümüşhane, Türkiye

INTRODUCTION

Analysis of regional and temporal behaviours of aftershock occurrences can be considered one of the significant tools for the understanding of earthquake mechanisms, because aftershock sequences supply potential information about the nucleation of earthquakes and physical characteristics of materials in the earthquake fault zone (Frohlich, Willemann 1987). Numerous aftershocks occur in a small region and in a short time and they are located in and around the mainshock in a small region and in a short time. Aftershock occurrences provide a detailed source of information on the Earth's crust, fault geometry, stress distribution and earthquake source properties following the mainshock as well as the aftershock hazard in comparison with mainshock hazard (Enescu, Ito 2002). Thus, aftershock sequences continue to exist as the key features of earthquake activity, and hence in recent years an increasing attention has been given

to the evaluation of aftershock sequences. Many statistical and physical models have been suggested to define the region-time-magnitude characteristics of aftershock occurrences, and a large number of analyses of the mainshock-aftershock pattern for different aftershock occurrences were achieved by different researchers (e.g., Utsu 1969; Wiemer, Katsumata 1999; Ogata 2001; Polat *et al*. 2002; Bayrak, Öztürk 2004; Helmstetter, Shaw 2006; Öztürk *et al*. 2008; Kayal *et al*. 2012; Hainzl *et al*. 2014; Adhikari *et al*. 2015; Wang *et al*. 2016; Özer, Polat 2017a, b; Wei-Jin, Jian 2017; Luginbuhl *et al*. 2018; Öztürk, Şahin 2019; Nanjo 2020; Sedghizadeh, Shcherbakov 2022).

Türkiye is one of the most seismo-tectonically active regions in the world. The movements in and around Türkiye result from the relative activities between different plate boundaries such as the African, Arabian, Aegean, Anatolian, Black Sea and Eurasian plates. Türkiye is located in the Mediterranean part of Alpine-Himalayan orogenic system, and the most significant tectonic structures can be given as the West Anatolian Extensional Zone (WAEZ), North Anatolian Fault Zone (NAFZ), East Anatolian Fault Zone (EAFZ), Central Anatolian Fault Zone (CAFZ), Bitlis Zagros Thrust Zone (BZTZ), East Anatolian Compressional Zone (EACZ), North East Anatolian Fault Zone (NEAFZ), Dead Sea Fault Zone (DSFZ), and Caucasus (Fig. 1a). The EAFZ in the south-eastern Türkiye, one of the main tectonic units, forms an active plate boundary between Arabia and Anatolia. The EAFZ is a 550 km long, approximately northeast trending sinistral strike-slip fault zone which includes a series of faults arranged parallel, subparallel or obliquely to the general trend. It shows a transform fault characteristic shaping from the boundaries between the Arabian and African plates and between the Anatolian and Eurasian plates (Westeway 1994). A conjugate structure to the NAFZ, the EAFZ extends from Karlıova in the northeast to Kahramanmaraş area in the southwest. It meets triple junctions with the NAFZ and forms the DSFZ (Bozkurt 2001). The EAFZ experienced many destructive earthquakes over historical times and these earthquakes caused damages and losses. Duman and Emre (2013) defined seven principle segments such as Erkenek (ErS), Pütürge (PtS), and Palu (PaS) along the strand of the EAFZ, and the largest one is the Pütürge segment, approximately 100 km long. A detailed active fault database including the EAFZ was provided from different sources such as Bozkurt (2001), Ulusay *et al*. (2004) and Emre *et al*. (2018). A great earthquake (with an intensity of Io = IX), which struck the Pütürge segment in Elazığ, with moment magnitude *M*w = 6.8 (local magnitude M_L = 6.6) at a depth of 4.8 km which has left a lateral strike slip faulting mechanism, occurred on 24 January 2020 between the southern Elazığ and Malatya provinces at local time 20:55:11.0 (17:55:11.0 UTC). According to the KOERI (Bogazici University, Kandilli Observatory and Earthquake Research Institute) records, the mainshock epicenter was given as 38.3775°N and 39.1042°E, located 0.81 km away from Çevrimtaş village in Elazığ-Sivrice. This earthquake provided some useful information to many researchers for the evaluation of earthquake potential in and around the EAFZ. This earthquake was one of the largest earthquakes that affected the EAFZ since 1971 (*M*6.8 Bingöl earthquake) and affected four cities in and around the mainshock region. The mainshock directly caused heavy damages and resulted in 41 causalities with hundreds of injured people. After the earthquake, 1540 buildings were damaged moderately, whereas 8519 buildings were collapsed or heavily damaged (Sayın *et al*. 2021).

The main purpose of this paper is to make an evaluation of the aftershock sequence following the 24 January 2020 M_W = 6.8 Elazığ-Sivrice earthquake. For this purpose, a comprehensive analysis in space, time and magnitude, including characteristic aftershock parameters such as the *b*-value in the Gutenberg-Richter formula, *p*-value in the modified Omori law, *Dc*-value in the fractal dimension, and Ma_{max} (possible maximum magnitude) value of aftershock occurrences, was achieved by using 4458 aftershocks described in one year from the mainshock. The *ZMAP* software package (Wiemer 2001) was used for all calculations of aftershock parameters. Since aftershock hazard after a mainshock are highly related to *b*-value, *p*-value and Ma_{max} value, the region-time-magnitude distribution of aftershock parameters may be important for the aftershock hazard evaluation. These types of characteristics of aftershocks can also supply preliminary information to appraise the hazard in the aftershock region.

DESCRIPTION OF THE CHARACTERISTIC AFTERSHOCK PARAMETERS

The region-time-magnitude distribution of aftershock sequences may supply quite effective preliminary and useful results on the variations of some parameters such as stress variations and coseismic deformation in the crust, fault structure, earthquake migration and distribution of cracks after the mainshock. Therefore, some characteristic aftershock parameters have been defined in magnitude (Gutenberg-Richter relation) (Gutenberg, Richter 1944), time (modified Omori model) (Utsu *et al*. 1995) and space (fractal dimension) (Grassberger, Procaccia 1983). These scaling laws are well known and the spatio-temporal distributions of aftershock sequences in different regions of the world were analyzed by many researchers mentioned above.

Gutenberg-Richter scaling law (*b*-value of magnitude-frequency relation)

The size-scaling relation defining the magnitude-frequency distribution of aftershock occurrences was given by Gutenberg, Richter (1944). This basic form is well known in earthquake statistics, and an empirical equation of this scaling law can be given as follows:

$$\log_{10} N(M) = a - bM \quad (1)$$

where *N (M)* is the cumulative number of aftershocks with magnitudes larger than or equal to *M*, *a*-value and *b*-value are positive constants. Variations in *a*-value depend on the observation period, size and seismicity of study region, and it exhibits important variations for different regions. The *b*-value defines the magnitude-frequency relation of aftershocks, and the tectonic structure of the study area affects the region-time changes in *b*-value. The *b*-value changes roughly between 0.6 and 1.4 (Wiemer, Katsumata 1999). Depending on the study area, Utsu (1971) also suggested that *b*-value changes mostly between 0.3 and 2.0. However, the average was described as close to 1.0 by Frohlich, Davis (1993). There exists a negative correlation between *b*-value and stress distribution, and the *b*-value shows the ratio between the relative numbers of small and large earthquakes (Scholz 2015). However, the physical meaning of the *b*-value is not clear and is still discussed.

Modified Omori law (*p*-value of aftershock decay rate)

The temporal aftershock decay rate can be described by a power law named as the modified Omori law or Omori-Utsu law (e.g., Utsu *et al*. 1995). According to the modified Omori law, the description of the aftershock decay rate with time following the mainshock can be provided by a scaling law as:

$$n(t) = \frac{K}{(t+c)^p} \quad (2)$$

where *n (t)* is the number of aftershocks (aftershock decay rate per day) per unit of time *t* (days) following the mainshock. *p*, *c*, and *K* values are positive constants. *c*-value and *K*-value depend on the activity rate in the earliest part of the sequence and the total number of aftershocks in the sequence, respectively. Stated as aftershock productivity, the *K*-value is controlled by the total number of aftershocks in the sequence. This normalizing parameter depends on the total aftershocks number and the threshold magnitude (Kisslinger, Jones 1991). The *c*-value is dependent on the aftershock activity rate in the earliest part of the sequences, and the missing detection of small events in the early stage of the sequence affects the estimation of *c*-value (Kisslinger, Jones 1991). The *p*-value is the most important among these parameters and defines the aftershock decay rate with time on frequency (Nanjo *et al*. 1998). A fast decay rate of aftershocks has a large *p*-value, but a slow decay of aftershock sequences has a small *p*-value. Many authors stated that *p*-value generally varies from 0.5 to 1.8 for different aftershock occurrences in the world (e.g., Olsson 1999; Wiemer, Katsumata 1999; Enescu, Ito 2002; Bayrak, Öztürk 2004; Öztürk, Şahin 2019). Variations in *p*-value may be associated with stress, fault heterogeneity, slip distribution and crustal heat flow but it is not clear which one is the most effective in *p*-value changes.

Fractal Dimension (*Dc*-value of earthquake distributions)

The fractal statement has been used for a long time to explain the complex fault systems. The fractal distribution of the earthquakes indicates that the number of events larger than a certain magnitude depends on the size as a power law. The concept of fractal geometry was introduced by Mandelbrot (1982) and extended by Turcotte (1992). Fault systems have a statistical self-similar structure in a wide range of size scales and are characterized by a power law named as fractal dimension, *Dc*-value. Thus, fractal dimension is widely preferred in seismology in order to analyze the regional distribution of epicentres. The correlation integral method is the most frequently preferred technique for the estimation of fractal dimension, and in the case of aftershock occurrences, this method measures the distance between two aftershock epicentres. Fractal dimension for the regional variation of aftershock distributions can be determined by using two-point correlation dimension, *Dc*, and correlation sum *C*(*r*) given by Grassberger, Procaccia (1983):

$$Dc = \lim_{r \to 0} \left[\log C(r) / \log r \right] \quad (3)$$

$$C(r) = 2N_{R<r} / N(N-1) \quad (4)$$

where *C* (*r*) is the correlation function, *r* is the distance between two aftershock epicentres, and *N* is the number of aftershock pairs separated by a distance $R < r$. The following formula is applied if the epicentre distribution has a fractal feature:

$$C(r) \sim r^{DC} \quad (5)$$

where *Dc* is the fractal dimension, more definitely, the correlation dimension. The distance *r* (in degrees) between two aftershocks is calculated from the following equation:

$$r = \cos^{-1} (\cos\theta_i \cos\theta_j + \sin\theta_i \sin\theta_j + \cos(\phi_i - \phi_j)) \quad (6)$$

where (θ_i, φ_i) and (θ_j, φ_j) are the latitudes and longitudes of the i^{th} and j^{th} aftershocks, respectively (Hirata 1989). The fractal dimension is computed by fitting a straight line by plotting $C(r)$ against r on a double logarithmic coordinate, and it is practically calculated from the slop of the straight line.

Earthquake distributions are accepted to be fractal, and fractal analysis based on the correlation integral can be used to analyze the regional distribution of the aftershock occurrences. Fractal dimension is related to the seismically and tectonically active regions and changes between 0 and 2 (Tosi 1998). If *Dc*-value is close to 0, it is considered that all aftershocks clustered into one point. If *Dc*-value is close to 1, it shows the dominance of line sources. If *Dc*-value is close to 2, it is suggested that the earthquake epicentres are homogeneously distributed over a two-dimensional fault plane (Hirata 1989; Öncel, Wilson 2002). Also, it is suggested that there is a negative correlation between *Dc*-value and *b*-value. A higher *Dc*-value associated with a lower *b*-value may be a dominant structural property in the regions of increased complexity in the active fault system. Therefore, it can be an evidence of stress variations in the region (Öncel *et al*. 1996; Öncel, Wilson 2002).

Aftershock sequence of the 24 January 2020 M_W = 6.8 Elazığ-Sivrice earthquake and organizing of the aftershock data

In this paper, a comprehensive assessment on the region-time-magnitude behaviours of the aftershock sequence of the 24 January 2020 Elazığ-Sivrice (Türkiye) earthquake (with a seismic moment of Mo = 1.387 × 10^{19} Nm, from U.S. Geological Survey) was carried out. The aftershock region was limited by taking into account the different studies as well the reports, and thus the area between the coordinates 38.3°E-39.7°E and 38.0°N-38.7°N was selected (Fig. 1a). Aftershock data was supplied from the Bogazici University, Kandilli Observatory and Earthquake Research Institute (KOERI). The mainshock was generated by the rupture of the PtS of the EAFZ, and the most earthquake-affected areas were Elazığ and Malatya provinces (Fig. 1b). The aftershocks of the 2020 Elazığ-Sivrice earthquake are distributed in an elliptical region and located between ErS and PaS in the NE-SW direction as seen in Fig. 1b. A dense aftershock activity in about one-year time interval from January 2020 to 31 December 2020 was observed after the mainshock. The main tectonic structures of the aftershock region and epicentre distributions of aftershocks with the mainshock are shown in Figs. 1b and 1c, respectively. The aftershock catalogue is homogenous for local magnitude, M_L, and consists of 4458 events with magnitudes $0.6 \leq M_L \leq 5.7$. For a detailed time-magnitude evaluation, the magnitude histogram and changes of aftershock magnitudes with time are plotted in Fig. 2. The magnitude histogram is given in Fig. 2a, and as seen in Fig. 2a, aftershock occurrences of the Elazığ-Sivrice earthquake are completed within the interval of M_L = 1.0–3.5. However, clear fluctuations can be seen in the number of aftershocks whose magnitudes change between 2.5 and 4.5 (Fig. 2b).

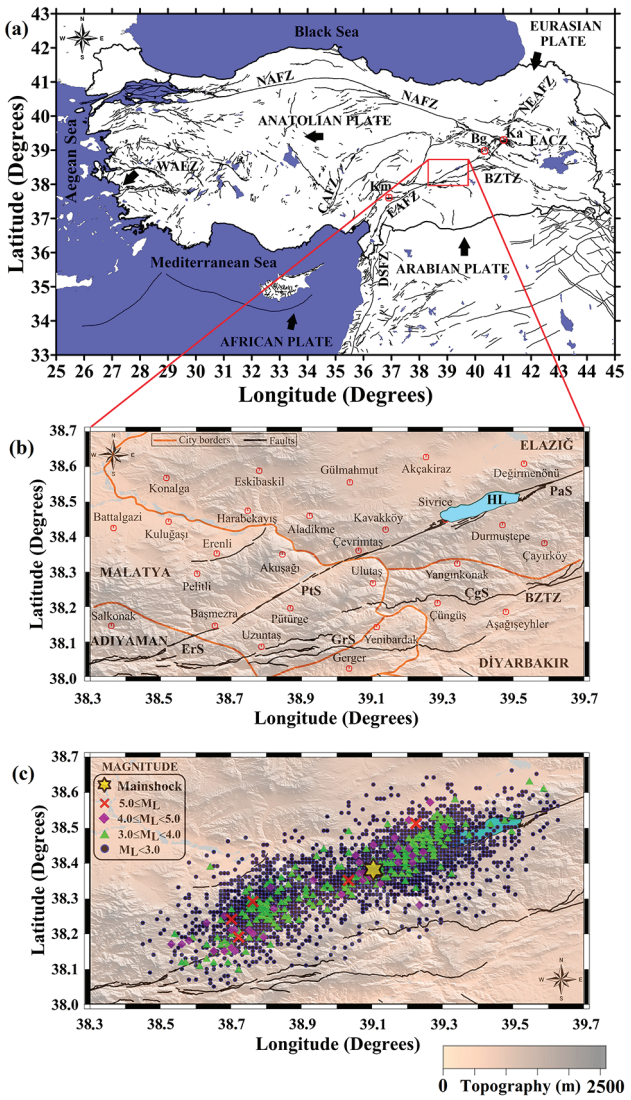

Fig. 1 (a) Simplified tectonic structure modified from Bozkurt (2001), Ulusay *et al*. (2004) and Emre *et al*. (2018). The red straight lines show the aftershock region. Abbreviations: *NAFZ*: North Anatolian Fault Zone, *WAEZ*: West Anatolian Extensional Zone, *CAFZ*: Central Anatolian Fault Zone, *EAFZ*: East Anatolian Fault Zone, *BZTZ*: Bitlis Zagros Thrust Zone, *NEAFZ*: North East Anatolian Fault Zone, *EACZ*: East Anatolian Compressional Zone, Ka: Karlıova, Bg: Bingöl, Km: Kahramanmaraş. (b) Tectonics of the aftershock region. Some residential centres were also shown on the Figure (*ErS*: Erkenek Segment, *PtS*: Pütürge Segment, *PaS*: Palu Segment, *ÇgS*: Çüngüş Segment, *GrS*: Gerger Segment, *HL*: Hazar Lake). (c) Aftershock epicentres of Elazığ-Sivrice earthquake. Mainshock is plotted with a star, and aftershocks are shown with different symbols

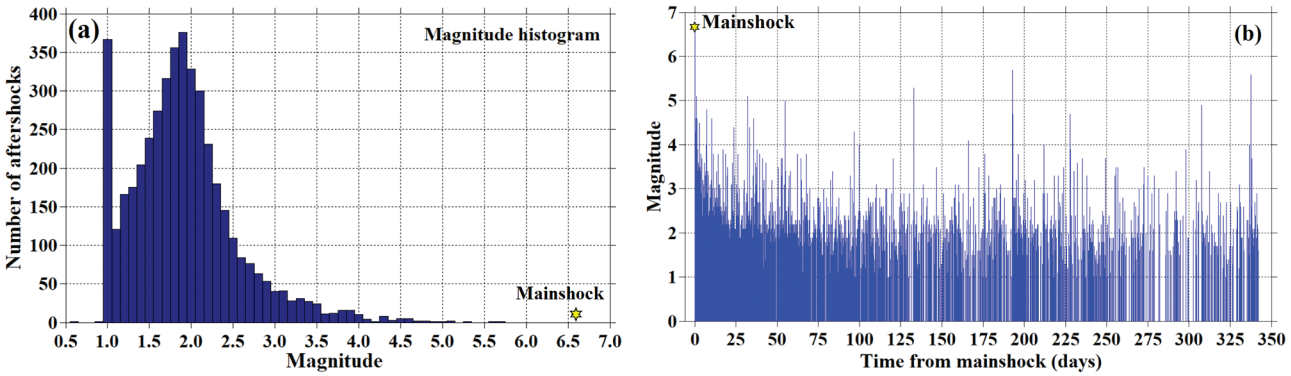

Fig. 2 (a) Magnitude histogram of aftershock sequence and (b) variations of aftershock magnitudes as a function of time

There are 4165 events with magnitude $M_L < 3.0$, 246 events with $3.0 \leq M_L < 4.0$, 41 events with $4.0 \leq M_L < 5.0$, 6 events with $M_L \geq 5.0$, and the aftershock with $M_L = 5.7$ is the biggest of all. The highest density of aftershocks (all size of events in general) was recorded in the whole parts of the aftershock region, while the larger aftershocks ($M_L \geq 4.0$) including the biggest event were especially recorded in and around the mainshock, in the northeast part of the mainshock and southwest end of the aftershock region (Fig. 1c).

In the aftershock-based analyses, the usage of a complete catalogue including all magnitude sizes is very important for the reliable results of characteristic aftershock parameters, especially in the calculation of *b*-value and *p*-value. Therefore, the maximum number of aftershocks is recommended to be used, and the first important stage must be considered to be the organizing of the minimum magnitude of completeness, *Mcomp*. This magnitude level can be simply defined as the lowest magnitude in the catalogue, and estimation of *Mcomp* is based on the assumption of G-R scaling law distribution of magnitudes. The *Mcomp* level includes 90% of the earthquakes that can be sampled with a scaling law (Wiemer, Wyss 2000) and shows spatio-temporal changes according to different networks and catalogues. The *Mcomp* value can be larger in the earliest part of the activity since the small events may not be recorded due to the first largest activity, and this a large *Mcomp* value causes the wrong evaluations of the characteristic aftershock parameters (Wiemer, Katsumata 1999). The changes in *Mcomp* value with time can be realized by using a moving time window approach with the maximum likelihood method (see Wiemer, Wyss 2000 for details). For the aftershock sequence of the Elazığ-Sivrice earthquake, starting at the mainshock time, a moving time window approach (given in ZMAP) was used. A sample time window length covering 40 aftershocks was considered to drawn the temporal changes of *Mcomp*, and fluctuations in *Mcomp* value with time are given in Fig. 3a. The largest *Mcomp* value was observed at the beginning of the sequence (for the first ten hours), and it changes between 2.5 and 3.4. Then it decreases to a value between 1.5 and 2.5 after two days following the mainshock. The *Mcomp* value shows a variation from 1.0 and 2.0, average *Mcomp* = 1.5, after 25 days following the mainshock. Thus, it can be stated that the *Mcomp* value in the aftershock sequence is not constant in the time period of one year. In addition to *Mcomp* variations with time, the regional changes of *Mcomp* value are also drawn in Fig. 3b. For the regional *Mcomp* map, the spatial grid cell spacing of 0.02° in longitude and latitude was used. As shown in Fig. 3b, the *Mcomp* value regionally varies from 1.0 to 2.1. The *Mcomp* value is mostly between 1.7 and 1.8 in the north-eastern and south-western parts of the aftershock area including ErS, PtS, GrS and PaS (north of Hazar Lake) whereas it changes from 1.0 to 1.5 between the mainshock epicentre and ÇgS (south of Hazar Lake). Considering *Mcomp* distribu-

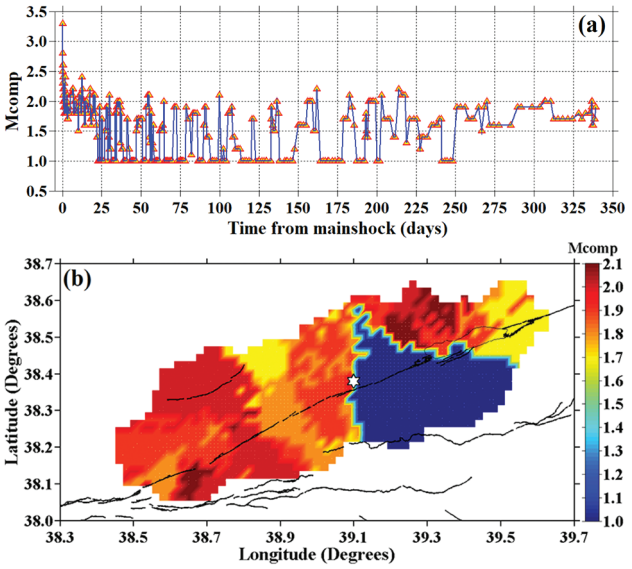

Fig. 3 (a) Changes in magnitude of completeness, *Mcomp*, as a function of time. *Mcomp* value was estimated with the moving time window technique, including 40 aftershocks. (b) Regional changes of *Mcomp* value. Star shows the mainshock

tion, it can be concluded that aftershock activity can be defined with a *Mcomp* value around 1.9 in many parts of the study area. Thus, the *Mcomp* value was considered to be 1.9 in the estimation of both *b*-value and *p*-value.

In the calculation of characteristic aftershock parameters, two fundamental inputs must be organized to ensure the completeness: (i) the minimum magnitude threshold, *Mmin*, and (ii) the minimum time threshold, *Tstart*, i.e. excluding the first hours to days from the mainshock. As a simple way, *Mmin* can be considered for the shortest *Tstart,* and thus this approach uses the biggest *Mcomp* value, described for the earliest part of the sequence (Wiemer, Katsumata 1999). However, the amount of available data is reduced with this application. For the aftershock sequence of the Elazığ-Sivrice earthquake, *Mmin* = 1.9 and *Tstart* = 0.01 were used to calculate the aftershock decay parameters. The *c*-value is measured in a time unit – days, for example. After some big earthquakes, some delay (usually small) can be seen in the aftershock sequences. It can be observed in the aftershock decay curve with time. In many cases, however, a large incompleteness can be seen in the catalogue at the earliest part of the aftershock sequence, and therefore an artificial large *c*-value can be computed. In fact, there is no upper limit of *c*-value. However, this value is generally suggested as small or very small: for example, around 0.01. In this study, by considering *Mmin* = 1.9 and *Tstart* = 0.01, it is aimed to remove these types of uncertainties on the estimations. With this approach, the earliest part of the sequence is included in the analyses, and completeness was provided although the number of aftershocks strongly decreased. Thus, in order to estimate the decay parameters of the modified Omori law, 2235 aftershocks with $M_L \geq 1.9$ were used.

In order to estimate the characteristic aftershock parameters, the ZMAP software package (Wiemer, 2001) was used. The *b*-value of the Gutenberg-Richter scaling law was estimated by the maximum likelihood method since it yields a more robust estimate than the least-square regression method (Aki 1965). The characteristic aftershock parameters of the modified Omori law were also estimated by the maximum likelihood method. The *Dc*-value of fractal dimension was computed in 95% confidence limits by the least squares method (Nanjo *et al*. 1998). The gridding technique was used for the regional demonstrations of *b*-value and *p*-value, and the nearest epicentres, *Ne*, were considered for each node of the grid (Wiemer, Wyss 1997; Wiemer, Katsumata 1999). This technique (Wiemer, Wyss 2000) determines the minimum threshold magnitude for which the goodness of fit is equal to and larger than 95%. If there is no such magnitude for the given confidence level, a 90% goodness of fit is assigned instead. However, the magnitude where the frequency-magnitude distribution has its maximum curvature is determined if the goodness of fit is less than 90% for any threshold magnitude. One of these magnitudes is assigned as the *Mcomp* value for that grid point. If the number of events with $M_L \geq Mcomp$ is larger than or equal to the minimum number of the nearest epicenters, *Nemin*, *b*-value and *p*-value are estimated for that node by using only the aftershocks with $M_L \geq Mcomp$. Finally, the regional imagines of *b*-value and *p*-value are mapped by the ZMAP software with the maximum likelihood approach.

Analyses of the characteristic aftershock parameters

A comprehensive evaluation of the characteristic aftershock parameters following the 24 January 2020 Elazığ-Sivrice earthquake was performed. In this context, region-time-magnitude analyses related to aftershock hazard assessment were achieved. Figure 4a shows the cumulative number of aftershocks in one year after the Elazığ-Sivrice mainshock. Considering the slope of the curve of the cumulative number of aftershocks, two subregions may be defined (Fig. 4a). The first two months can be considered as the first part, and the rest ten months as the second region. 2537 aftershocks were recorded in the first two months from the mainshock, and a total of 1921 aftershocks in the remaining time period. Aftershock activity after the first two months is relatively constant and it indicates a slower decrease compared to the activity of the first two months. The time histogram of aftershock sequence in one year is presented in Fig. 4b. As shown in the variations of the number of aftershocks, aftershock activity in the first two months shows a denser occurrence, whereas a more constant activity was recorded after the first 60 days following the mainshock. Although there are some fluctuations in the activity in different times, it can be clearly seen from Fig. 4b that aftershock activity comes to an end after one year. As stated in Tajima and Kanamori (1985), the duration of aftershocks for large mainshocks may extend one year. Tsapanos *et al*. (1994) suggested that an event may be considered an aftershock if it occurs between 100 and 150 days from the mainshock. For different aftershock occurrences, many researchers considered different time periods; for example, one month by Öztürk *et al*. (2008), four months by Enescu, Ito (2002), five months by Bayrak, Öztürk (2004), and six months by Nuannin *et al*. (2012) and by Öztürk, Şahin (2019). Considering these studies and the temporal distribution of aftershocks showed in Figs 4a and 4b, the aftershock activity for the 24 January 2020 Elazığ-Sivrice earthquake was cut in a one-year time period.

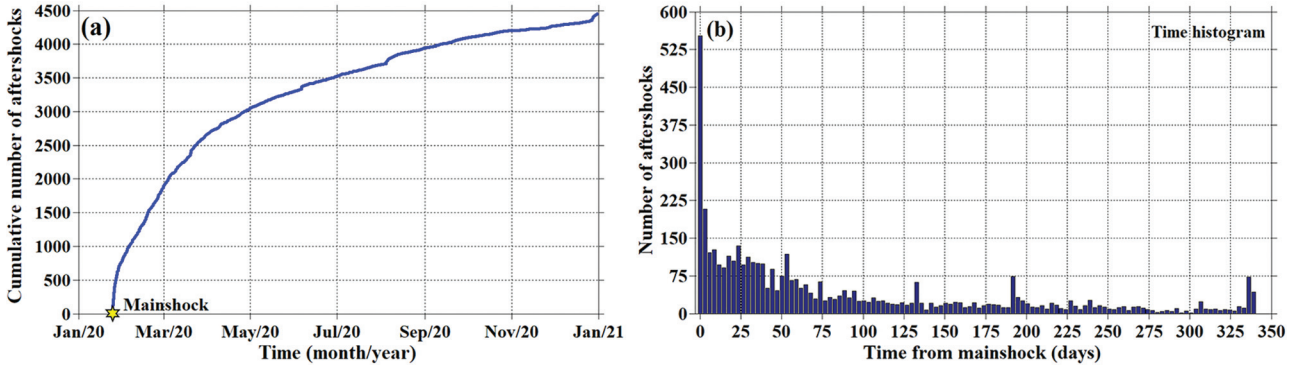

Fig. 4 (a) Cumulative number of aftershock in one year following the mainshock. (b) Time histogram of aftershock sequence

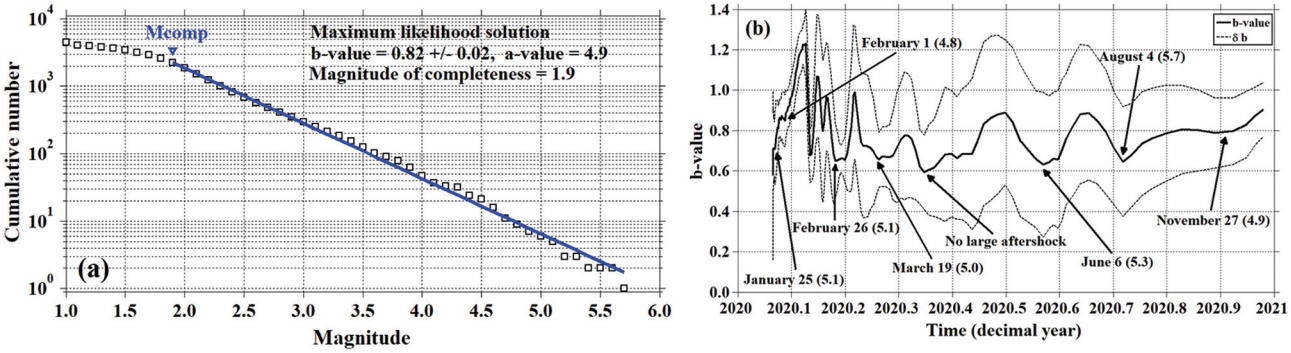

Fig. 5 (a) Gutenberg-Richter relation and magnitude-frequency distribution of aftershock sequence; *b*-value, its standard deviation, *Mcomp* value and *a*-value are given. (b) *b*-value changes as a function of time following the mainshock. Arrows indicate sudden decreases in *b*-value before larger aftershock occurrences

The Gutenberg-Richter relation showing the magnitude-frequency distribution of aftershock sequence is given in Fig. 5a. The *Mcomp* value was taken as 1.9 by considering regional and temporal changes presented in Fig. 3, and the *b*-value was estimated as 0.82 ± 0.02 by using the maximum likelihood solution. This *b*-value is relatively smaller than the average *b*-value of 1.0 which is observed worldwide. However, as seen in Fig. 5a, the magnitude-frequency distribution of the Elazığ-Sivrice aftershock sequence is well represented by the Gutenberg-Richter scaling law with an average *b*-value close to 1.0. Frochlich, Davis (1993) suggested that some factors such as a higher stress concentration, high strain in the region, or low heterogeneity degree of medium can cause decreases in *b*-value. Bender (1983) provided a detailed study on the dependence of the *b*-value on the data fitting techniques, relative number of small and large earthquakes, maximum magnitude in the catalogue, interval size, and sample size. A low *b*-value is related to a great number of large earthquakes, whereas a high *b*-value indicates that there are many small earthquakes rather than great earthquakes in the catalogue. As given above in a section on aftershock data, there are 246 aftershocks with $3.0 \leq M_L < 4.0$ and 47 aftershocks with $M_L \geq 4.0$. Thus, this low *b*-value may be related to a relatively large number of aftershocks with $M_L \geq 4.0$. Variations in *b*-value within one year after the mainshock of the Elazığ-Sivrice earthquake are also given in Fig. 5b. As in the calculation of the *Mcomp* value, the moving time window approach and the maximum likelihood estimation were used for the estimation of temporal *b*-value changes, and a sample size of 150 aftershocks was considered. As shown in Fig. 5b, the *b*-value varies in a large band between 0.6 and 1.2. Following the mainshock, there are remarkable decreases and increases in *b*-value as a function of time. The times of the occurrences and their magnitudes for the largest aftershocks are given with the arrows on Fig. 5b. It can be clearly seen from Fig. 5b that rapid decreases in *b*-value are related to the occurrence times of the largest aftershocks, while the sudden increases were found after the occurrences of the largest aftershocks. The *b*-value variations, however, have an average value of 0.8. As stated above, several factors can cause perturbations of the normal *b*-value. It can be interpreted that temporal decreases in *b*-value before the larger aftershocks may have resulted from a stepwise increase in the effective stress. Also, a rapid increase in the temporal *b*-value may be due to the reduced stress in these times following the larger aftershocks. Hence, the assessment of temporal changes in *b*-value may be accepted as a significant tool for aftershock hazard.

The modified Omori law fit to the cumulative numbers of aftershock sequence was observed from the mainshock time of the 24 January 2020 Elazığ-Sivrice earthquake, and the estimated aftershock decay parameters for different starting times with the magnitudes *Mcomp* ≥ *Mmin* are plotted in Fig. 6. All aftershock parameters including *p, c* and *K*-values in the modified Omori formula, their standard deviations, minimum magnitude, starting time for the data, and the number of aftershocks are also given. For the calculation of *p*, *c* and *K*-values, the maximum likelihood approach was used, and the aftershock sequence was modelled by the modified Omori model, closely following the modified Omori law with a clear exponential decay. The *p*-value was calculated as 0.72 ± 0.01 with *c*-value = 0.727 ± 0.146 assuming *Mmin* = 0.6 (including all 4458 aftershocks) starting from the mainshock time (Fig. 6a). The *p*-value was computed as 0.80 ± 0.02 for the sequence by using *Mmin* = 1.9 and *Tstart* = 0.01 with *c*-value = 0.279 ± 0.068 (Fig. 6b). Also, the *p*-value was estimated as 0.80 ± 0.02 with *c*-value = 0.277 ± 0.066 by considering *Mmin* = 1.9 beginning at the mainshock time (Fig. 6c). Mogi (1962) suggested a relation among the *p*-value, structural heterogeneity, stress, and temperature in the crust (*p*-value increases with increasing temperature). According to Dieterich (1994), if the main shock is modelled as a dislocation, the aftershock rate within a finite time interval and region decays with the *p*-value about 0.8, due to a non-uniform stress change around the mainshock. Helmstetter *et al*. (2005) found that the *p*-value is close to 0.9 for times between less than a minute and one year for the stacked aftershock sequences in Southern California. Also, Helmstetter and Shaw (2006) stated that a heterogeneous stress distribution produces a power law decay with a *p*-value smaller than 1.0 (the more heterogeneous the stress is, the larger the *p*-value is (closer to 1). Peng *et al*. (2007) observed *p*-value = 0.92 ± 0.04 for long-term aftershocks and stated that this value is close to the aftershock decay rate of $p \sim 0.8$ for a finite region surrounding a shear crack (Dieterich 1994). According to these results, there is a low stress heterogeneity in the Elazığ-Sivrice aftershock sequence. A smaller *p*-value for an aftershock occurrence also indicates a slow decay rate, and thus the aftershocks sequence of the Elazığ-Sivrice earthquake has a relatively slow decay rate (as seen in Figs. 4a and 4b). It is stated that the superposed sequences contain usually small aftershocks and a portion of these events may not be real aftershocks; they may only relate to the background seismicity (Utsu *et al*. 1995). As stated above in a section on aftershock data, there are 4165 aftershocks with $M_L < 3.0$ in the sequence of the Elazığ-Sivrice earthquake. Also, the catalogue including the first two months has 2537 aftershocks. The effects of different *Mmin* and *Tstart* values were tested for the confidence of *p*- and *c*-values. All results are presented in Table 1. The *p*-value is independent of *Mmin* (Utsu *et al*. 1995), but the *c*-value depends strongly on the *Mmin* value. Some tests were provided for the decay parameters using different *Mmin* (ranging from 1.9 to 2.6) and *Tstart* (ranging from 0.006 to 0.1) values. The *p*-value changes between 0.78 and 0.86 for different *Mmin* and *Tstart* values, and the *c*-value varies from 0.0 to 0.294. Thus, the *c*-value is related to the minimum magnitude in comparison with the *p*-value.

In order to analyse the aftershock behaviours as a scaling law after the first definition by Omori (1984), several models have been suggested to measure, map and evaluate the decay rate of aftershock activity. Different techniques such as Epidemic Type Aftershock Sequence (ETAS) model (Ogata 1983), Marcellini (1997) approach, stretched exponential relaxa-

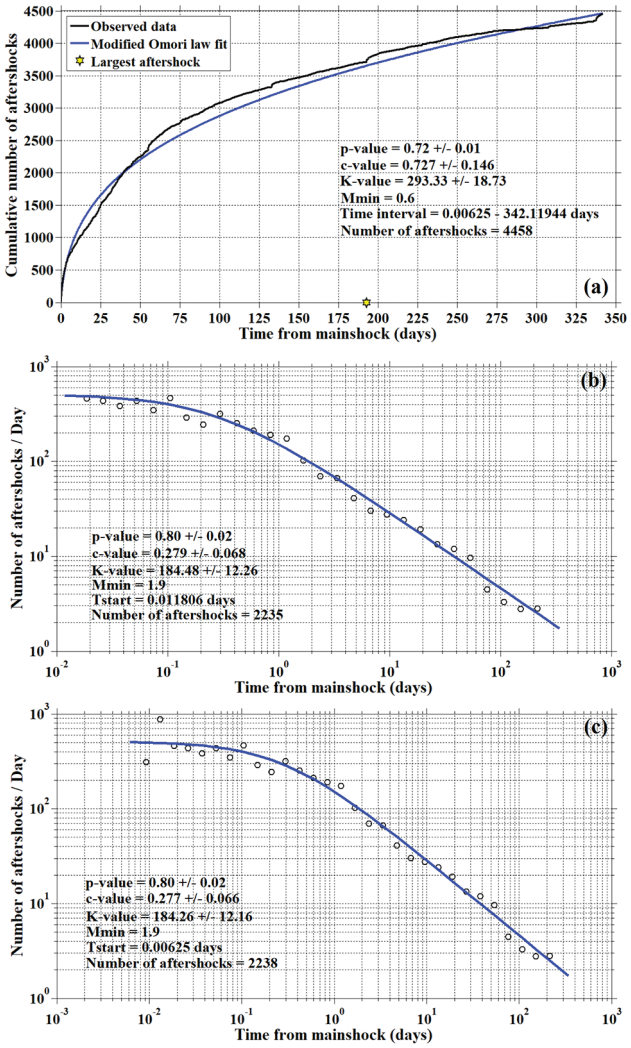

Fig. 6 (a) The modified Omori law fit to the observed data starting from mainshock time (for the cases: $M_L \geq 0.6$). (b) Aftershock decay parameters starting 0.01 days after the mainshock (for the cases: $M_L \geq 1.9$, No: 1 in Table 1). (c) Aftershock decay parameters starting from mainshock time (for the cases: $M_L \geq 1.9$, No: 21 in Table 1)

Table 1 Results of detailed tests for the estimation of characteristic aftershock parameters with different input parameters

No	Minimum time threshold (*Tstart*, days)	Minimum magnitude threshold *Mmin*	Time interval (*t*, days)	Number of aftershocks	*p*-value	*c*-value	*K*-value
1	**0.01**	**1.9**	**0.011806 ≤ *t* ≤ 341.6583**	**2235**	**0.80 ± 0.02**	**0.279 ± 0.068**	**184.48 ± 12.26**
2	0.01	2.0	0.011806 ≤ *t* ≤ 341.6583	1859	0.81 ± 0.02	0.204 ± 0.055	152.54 ± 10.28
3	0.01	2.1	0.011806 ≤ *t* ≤ 341.6583	1531	0.82 ± 0.02	0.154 ± 0.046	127.97 ± 8.84
4	0.01	2.2	0.011806 ≤ *t* ≤ 341.4514	1231	0.83 ± 0.02	0.109 ± 0.036	103.57 ± 7.36
5	0.01	2.3	0.011806 ≤ *t* ≤ 341.1847	1000	0.83 ± 0.02	0.082 ± 0.031	84.9 ± 6.29
6	0.05	1.9	0.051389 ≤ *t* ≤ 341.6583	2215	0.80 ± 0.02	0.294 ± 0.080	185.84 ± 12.97
7	0.05	2.0	0.051389≤ ≤ *t* ≤ 341.6583	1839	0.81 ± 0.02	0.212 ± 0.067	153.23 ± 10.91
8	0.05	2.1	0.051389 ≤ *t* ≤ 341.6583	1511	0.82 ± 0.02	0.156 ± 0.057	128.2 ± 9.41
9	0.05	2.2	0.051389 ≤ *t* ≤ 341.4514	1211	0.83 ± 0.02	0.105 ± 0.047	103.3 ± 7.86
10	0.05	2.3	0.051389 ≤ *t* ≤ 341.1847	980	0.83 ± 0.02	0.078 ± 0.043	84.68 ± 6.81
11	0.1	1.9	0.10486 ≤ *t* ≤ 341.6583	2196	0.80 ± 0.02	0.262 ± 0.086	183.23 ± 13.09
12	0.1	2.0	0.10486≤ ≤ *t* ≤ 341.6583	1820	0.80 ± 0.02	0.179±0.073	150.6 ± 11.01
13	0.1	2.1	0.10486 ≤ *t* ≤ 341.6583	1492	0.81 ± 0.02	0.120 ± 0.063	125.36 ± 9.48
14	0.1	2.2	0.10486 ≤ *t* ≤ 341.4514	1192	0.82 ± 0.02	0.069 ± 0.054	100.61 ± 7.95
15	0.1	2.3	0.10486 ≤ *t* ≤ 341.1847	962	0.83 ± 0.02	0.038 ± 0.049	81.81 ± 6.84
16	0.5	1.9	0.50486 ≤ *t* ≤ 341.6583	2082	0.78 ± 0.02	0.057 ± 0.14	169.35 ± 14.15
17	0.5	2.0	0.50486 ≤ *t* ≤ 341.6583	1714	0.79 ± 0.02	0.0 ± 0.137	141.21 ± 12.56
18	0.5	2.1	0.50833 ≤ *t* ≤ 341.6583	1391	0.81 ± 0.02	0.0 ± 0.147	120.95 ± 11.87
19	0.5	2.2	0.50833 ≤ *t* ≤ 341.4514	1101	0.82 ± 0.03	0.0 ± 0.159	100.77 ± 11.03
20	0.5	2.3	0.50833 ≤ *t* ≤ 341.1847	878	0.83 ± 0.03	0.0 ± 0.175	82.34 ± 10.06
21	–	**1.9**	**0.00625 ≤ *t* ≤ 341.6583**	**2238**	**0.80 ± 0.02**	**0.277 ± 0.066**	**184.26 ± 12.16**
22	–	2.0	0.00625 ≤ *t* ≤ 341.6583	1862	0.81 ± 0.02	0.204 ± 0.053	152.46 ± 10.19
23	–	2.1	0.00625 ≤ *t* ≤ 341.6583	1534	0.82 ± 0.02	0.155 ± 0.044	127.98 ± 8.77
24	–	2.2	0.00625 ≤ *t* ≤ 341.4514	1234	0.83 ± 0.02	0.111 ± 0.035	103.72 ± 7.31
25	–	2.3	0.00625 ≤ *t* ≤ 41.1847	1003	0.84 ± 0.02	0.084 ± 0.03	85.08 ± 6.24
26	–	2.4	0.00625 ≤ *t* ≤ 341.1847	823	0.86 ± 0.02	0.076 ± 0.028	73.44 ± 5.71
27	–	2.5	0.00625 ≤ *t* ≤ 341.1847	678	0.86 ± 0.02	0.051 ± 0.022	59.2 ± 4.71
28	–	2.6	0.00625 ≤ *t* ≤ 341.1847	569	0.86 ± 0.02	0.037 ± 0.018	48.82 ± 4.01

tion (Mignan 2015), modified Omori law including a background rate term (Öztürk *et al*. 2008), etc., have been proposed to analyze the aftershock decay rate. However, these applications have limited results relative to the modified Omori law. Therefore, the modified Omori model is one of the most applicable methods, and time series analyzes of aftershocks in the present study fit well with the modified Omori law. Considering the detailed tests given in Table 1, the modified Omori model appears suitable for the estimation of aftershock decay parameters of the Elazığ-Sivrice aftershock sequence.

If the smaller aftershocks are frequently hidden by larger events because of the overlapping, aftershock numbers may not be counted fully at the early stage of the sequence and hence relatively great *c*-values may be obtained. If all aftershocks may be counted, the *c*-value may be zero (Utsu 1971). Two approaches may be given in relation to the *c*-value: one is that *c*-value is actually 0, and all the estimated positive *c*-values are related to incompleteness at the beginning of an aftershock sequence. The second opinion is that a positive *c*-value can be estimated (Enescu, Ito 2002). If *c*-value equals 0, *n (t)* in Equation (2) diverges at the mainshock time ($t = 0$). If the expansion of the aftershock area occurs in an early stage, a relatively high *c*-value may be estimated (Utsu *et al*. 1995). Also, for the aftershock occurrences following relatively small mainshocks, *c*-values are generally estimated as smaller than ≤ 0.01 days. Considering the detailed literature studies given above, it can be concluded that the use of *Mmin* = 1.9 and *Tstart* = 0.01 (for the cases No: 1 in Table 1, also Fig. 6b) for the estimation of aftershock decay parameters appears better to fit the Elazığ-Sivrice aftershock sequence, and the results are compatible with other literature studies. In addition, obtained results suggest that there is no heterogeneous background seismicity pattern in the aftershock activity. As a remarkable fact, the simple modified Omori law seems very suitable in the description of the aftershock decay parameters in the Elazığ-Sivrice sequence.

The *Dc*-value of aftershock epicentre distributions for the Elazığ-Sivrice earthquake is plotted in Fig. 7. As shown in Fig. 7, a straight line fitted the curve of the mean correlation integral against the distance

of events, R (km). Considering the 95% confidence interval by the least square approach, *Dc*-value was estimated as 1.87 ± 0.07 for epicentre distributions of 4458 aftershocks. This log-log relation has a clear linear range and scale invariance in the self-similarity statistics between 4.84 and 21.76 km (indicated in Fig. 7 as "Range"). This range changes mostly between 5 and 10 km in space and time for the epicentres of Türkiye earthquakes. Thus, the minimum range value (*Rmin* = 4.84 km) considered for the calculation of the *Dc*-value in this work is in compliance with literature. The fractal dimension, as stated above, can be used as a quantitative measure of heterogeneity degrees in fault geometry and stress (Öncel *et al*. 1996; Öncel, Wilson 2002). If an active fault system has an increasing complexity with a larger *Dc*-value and a lower *b*-value, the stress release occurs on fault planes of a smaller surface area (Öncel, Wilson 2002). In addition, a higher *Dc*-value is sensitive to heterogeneity in magnitude variations. The *Dc*-value estimated as 1.87 ± 0.07 for the aftershocks distribution implies that aftershocks are more clustered at larger scales or in smaller areas. It can be considered that Elazığ-Sivrice aftershocks have a homogeneous distribution on a two dimensional fault plane since the *Dc*-value is close to 2.0. In addition, the heterogeneity degree of earthquake activity can be measured quantitatively considering the fractal dimension, and the heterogeneity of stress field dominates the region (Öncel *et al*. 1996). Therefore, it can be interpreted as a non-heterogeneous stress distribution in Elazığ-Sivrice region. Thus, we can statistically describe and characterize the spatial distributions of aftershock epicentres and their fracture systems with fractal dimension. Considering the negative correlation between *Dc*-value and *b*-value, a larger *Dc*-value (1.87 ± 0.07) associated with a smaller *b*-value (0.82 ± 0.02) can be considered a dominant structural property for the aftershock area with the increasing complexity in the active fault system. Hence, it can be considered to be evidence of stress changes in the aftershock area (Öncel *et al*. 1996; Öncel, Wilson 2002).

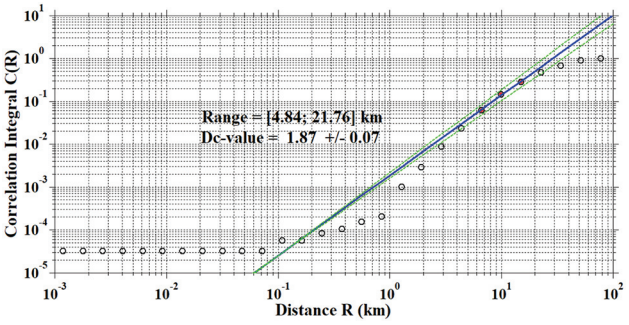

Fig. 7 Fractal dimension of epicentre distributions, *Dc*-value, for Elazığ-Sivrice aftershock sequence

Regional variations of *b*-value, *p*-value and Ma_{max} value

The procedure that is explained above in a section on aftershock data was applied to obtain regional changes of *b*-value and *p*-value. The aftershock area was divided into rectangular cells separated by 0.02° in latitude and longitude. The nearest epicentres (number of events, *Ne*) were taken as 350 aftershocks for each cell, and the minimum nearest epicentres (*Nemin*, minimum number of events > *Mcomp*) were taken as 100 events. Then, the regional changes of *b*-value and *p*-value were mapped considering the number of aftershocks between 100 and 350. Next, as an important input data, *c*-value was taken as 0.279 days and *Tstart* = 0.01 days since these input parameters are more satisfying (the first calculation in Table 1 and Fig. 6b) for the regional imaging of *p*-value. Considering the region-time variation in *Mcomp* value (Figs 3a and 3b), it was accepted as around 1.9 for most of the cells. Then, this value was used by ZMAP as *Mcomp* for all grid cells. If the number of aftershocks with $M_L \geq Mcomp$ is larger than or equal to *Nemin* in each cell, *b*-value and *p*-value are calculated for each cell by using only the aftershocks with $M_L \geq Mcomp$. As a result, the regional changes of *b*-value and *p*-value were mapped by using *Ne* = 350 with Ne_{min} = 100 aftershocks for the Elazığ-Sivrice aftershock sequence.

The regional distributions of *b*-value and *p*-value for the Elazığ-Sivrice aftershock sequence are shown in Figs 8 and 9, respectively. The *b*-value shows a regional variation between 0.5 and 1.2, and regional changes in *p*-value vary from 0.5 to 1.1. These change intervals in *b*-value and *p*-value are compatible with the literature studies mentioned above, such as Utsu (1971), Wiemer, Katsumata (1999), Enescu, Ito (2002), Öztürk, Şahin (2019), etc. The aftershock activity of the Elazığ-Sivrice earthquake (including all sizes of aftershocks with $M_L < 5.0$) densely occurred in and around the mainshock, in the north-eastern and south-western parts of the mainshock (Fig. 1c). Also, the largest aftershocks with $M_L \geq 5.0$ show a high density around the mainshock epicentre and in the south-western end of the sequence. The *b*-value changes can be thought to form three groups: (*i*) the smallest *b*-values (< 0.8) in the north and south direction from the mainshock epicentre (including Gülmahmut, Akçakiraz, Sivrice, Ulutaş, Çevrimtaş, and Kavakköy) and in the south-western end of the region (including Erkenek segment, Pütürge, Uzuntaş, Başmezra, and Pelitli), (*ii*) intermediate *b*-values (between 0.9 and 1.1) in the northwest and southeast direction from in Pütügre segment (including Harabekayış, Akuşağı, Aladikme, Yangınkonak,

and the north and south parts of Hazar Lake), and (*iii*) the highest *b*-values (>1.1) in the northeast end of the region (including Değirmenönü, Durmuştepe, and Çayırköy). The smaller *b*-values were generally computed in the larger aftershock ($M_L \geq 4.0$) regions, while the highest *b*-values are related to the regions in which aftershocks with $M_L < 3.0$ are generally observed. The regional variations of *p*-value for the Elazığ-Sivrice aftershock sequence have both low and high values in the whole aftershock area. The largest *p*-values (> 1.0) were found in the north and south parts of the mainshock epicentre (in and around the mainshock including Ulutaş, Çevrimtaş, Kavakköy, and Aladikme), and there is a faster decay of aftershock activity in these areas. On the contrary, lower *p*-values (< 0.7) were obtained in the south parts of the Hazar Lake, northwest part of Pütürge segment, and southwest end of the aftershock region (including Durmuştepe, Çakırköy, Yangınkonak, Erkenek segment, Başmezra, Pelitli, and Erenli). These small *p*-values means that the aftershock decay rate is slower in these parts rather than in other parts of the region. Thus, aftershock activity decays faster in and around the mainshock epicentre ($p \sim 1.1$) than along other parts.

One of the most important estimations in these types of studies is to define the occurrence of the aftershock with the maximum magnitude (Ma_{max}).

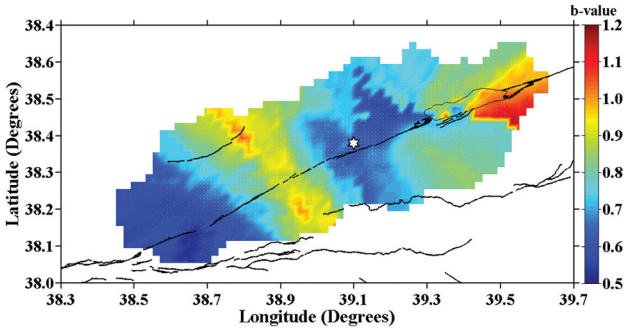

Fig. 8 Regional changes of *b*-value. *b*-value is plotted by sampling the nearest 350 aftershocks with cells spaced 0.02° in latitude and longitude. Star shows the mainshock

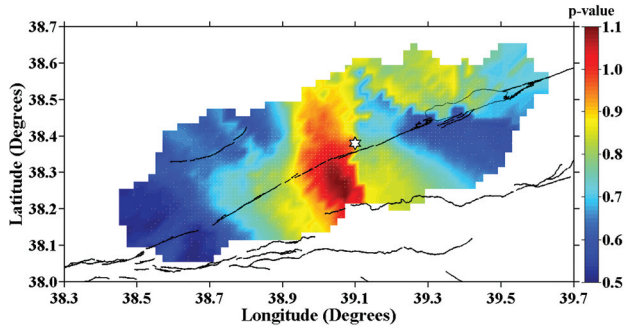

Fig. 9 Regional changes of *p*-value. *p*-value is plotted by using the same grid and number of aftershocks with cells spaced as in the case of *b*-value map. Star shows the mainshock

Therefore, a possible Ma_{max} value after the Elazığ-Sivrice mainshock was regionally tried to be estimated. On a global scale, the average difference between mainshock magnitude and the largest aftershock magnitude is suggested as constant and equal to 1.2 (Båth 1965). However, for Türkiye earthquakes, this difference was suggested as 0.9 by using the Gutenberg-Richter relationship (Öztürk 2009). The regional changes of Ma_{max} value for the Elazığ-Sivrice aftershock sequence are given in Fig. 10. The Ma_{max} value changes between 3.3 and 5.7. Larger Ma_{max} values (> 4.8) were found in and around the mainshock, southeast end of the region, northwest of Pütürge segment, and in the northwest direction from Hazar Lake (including Çevrimtaş, Ulutaş, Akuşağı, Pütürge, Uzuntaş, Başmezra, Erkenek segment, Pelitli, Erenli, Akçakiraz, and Sivrice), whereas smaller Ma_{max} values (< 4.0) were calculated between Hazar Lake and Çüngüş segment (including Durmuştepe, Çayırköy, and Yangınkonak). As seen from Figs 8 and 10, there exists a clear relation between the smallest *b*-values and largest Ma_{max} values. In addition, considering the difference between the mainshock and the largest aftershock magnitudes as 0.9 according to Öztürk (2009), a possible largest Ma_{max} value can be considered to be 5.7. Thus, as seen in Fig. 10, this result is very compatible with the Ma_{max} value in the present study. A study including estimation of the maximum magnitudes in aftershock sequences was conducted by Chan and Wu (2013). They proposed that, once a database for the regional changes of *b*-values is estimated, the possible maximum aftershock magnitude can be calculated immediately following the mainshock. They also suggested that this type of evaluations can supply preliminary results for the estimation of seismic hazard. Also, Öztürk, Şahin (2019) made a statistical region-time-magnitude evaluation on the aftershocks occurrence of the 21 July 2017, *M*w = 6.5, Bodrum-Kos, Türkiye, earthquake. They suggested a clear correlation between a low *b*-value and a high Ma_{max} value. This type of calculations may be applied to determine the possible location of the

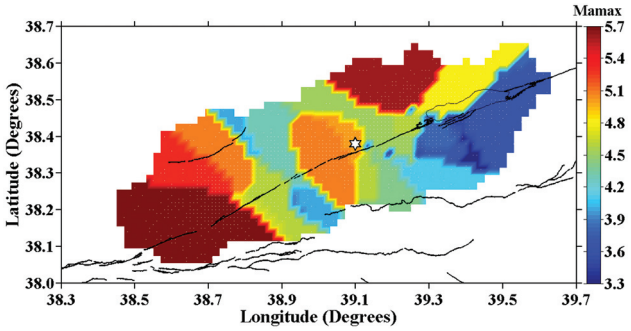

Fig. 10 Regional changes of the maximum aftershock magnitude, Ma_{max}. Ma_{max} value is plotted by using the same grid and number of aftershocks with cells spaced as in the case of *b*-value and *p*-value maps. Star shows the mainshock

next strong aftershocks, since a fast evaluation of a short-term aftershock hazard shortly after a strong/large earthquake may give clues on the destruction assessments or urgent intervention. Therefore, a special interest must be given to the regions where the largest Ma_{max} values were calculated.

Some comments on the regional changes of *b*-value and *p*-value

Large or destructive earthquakes always generate many aftershocks, and after the main rupture is completed, interaction of faults and stresses have a significant impact on the aftershock occurrence. From the previous studies given above, there exists a clear relation between the characteristic aftershock parameters and structural properties of the aftershock region, since the region-time-magnitude variations of aftershock sequences include some useful information about the earthquake nucleation, fault geometry, the physical properties of the materials in the fault zone, distributions of slip, stress and temperature (Kisslinger, Jones 1991). There are many studies on the regional and temporal evaluation of aftershock sequences of mainshocks from Turkey and different parts of the world (e.g., Kisslinger, Jones 1991; Wiemer, Katsumata 1999; Enescu, Ito 2002; Bayrak, Öztürk 2004; Öztürk *et al*. 2008; Wang *et al*. 2016; Öztürk, Şahin 2019; Nanjo 2020; Öztürk 2021) and these researchers suggested that regional changes in *b*-value and *p*-value are controlled by rupture mechanisms during the mainshock, and the variations in these parameters are related to the material properties of the aftershock area. According to their results, the areas with a smaller *b*-value are related to the regions with a lower stress after the mainshock, and the regions with a higher *p*-value are related to the areas that the experienced higher coseismic slip distribution after the mainshock. Öztürk, Şahin (2019) summarized the general results of these studies as follows: (1) regional and temporal changes in these parameters show a good relation to the tectonic properties and/or some variables of the earthquake occurrences, (2) the most characteristic element controlling the regional changes on these parameters is probably the fault slip, (3) the region-time variations of these parameters supply statistically significant information for practical forecast, (4) aftershock effects can be used to determine the nonlinear seismic response and accumulated damage of concrete gravity dams, (5) the regional variations of the aftershock parameters correspond quite well to the causative fault planes of earthquakes, (6) estimation of characteristic aftershock parameters may serve for a rapid evaluation of a short-term earthquake hazard immediately after the large/devastating earthquakes, and (7) the region-time-magnitude analysis of aftershock sequences may provide rapid evaluation of mainshock-induced stress fields and may forecast the aftershock with maximum magnitude triggered by the mainshock.

Following the 24 January 2020 Elazığ-Sivrice (Türkiye) earthquake, several studies including geotechnical evaluations were made. For this purpose, different parameters such as coseismic slip distribution and displacement, postseismic deformation, mainshock faulting, rupture kinematics, dynamic modelling and stress distribution were analyzed and discussed (e.g., Cheloni, Akinci 2020; Chen *et al*. 2020; Pousse-Beltran *et al*. 2020; Sayın *et al*. 2021; Lin *et al*. 2021; Bayrak, Özer 2021; Alkan *et al*. 2021). The 24 January 2020 Elazığ-Sivrice earthquake caused loss of life and important seismic damage to buildings in the epicentral region. The effects of the mainshock on the structures was quite serious although the mainshock was moderate. After the end of the seismic quiescence period that started in 1971, this earthquake struck the PtS in Elazığ and supplied valuable insights to the researchers in order to reinterpret the earthquake potential along the EAFZ and its surroundings. Therefore, interrelationships between characteristic aftershock parameters and other geophysical parameters analyzed by given authors may contribute to the assessment of aftershock hazard after the Elazığ-Sivrice mainshock.

Cheloni, Akinci (2020) made an analysis to model the main features of the rupture process and the strong ground motion during the Elazığ earthquake. They used Interferometric Synthetic Aperture Radar (InSAR) interferograms to restrict the fault geometry and the coseismic slip distribution of the causative fault segment (see their Figs 2, 3 and 4). They also used this information to analyze the ground motion characteristics of the mainshock in terms of peak ground acceleration (PGA), peak ground velocity (PGV) and spectral accelerations (see their Fig. 7). Their results show that the 2020 Elazığ earthquake ruptured two main slip patches (for a total length of about 40 km) located along PtS. Their another calculation including Coulomb stress distribution provides that the Elazığ mainshock increased the stress level of the westernmost part of Pütürge fault and of the following PaS (see their Fig. 12). As discussed in Section 5 of their article, these areas are related to the lower *b*-values, higher *p*-values and the largest Ma_{max} values. Thus, these results are consistent with the findings of other researchers mentioned above.

Chen *et al*. (2020) investigated the rupture kinematics of the 24 January 2020 Elazığ earthquake from joint inversion of InSAR interferograms, strong motion, and broadband teleseismic *P* waveforms (see their Fig. 2). They performed dynamic rupture simulations to provide a physically reasonable rup-

ture process based on the stress drop inferred from the kinematic model (see their Fig. 3). In addition, they calculated Coulomb stress failure, and their dynamic model shows an initial heterogeneous stress distribution with variations up to 30 MPa, which was probably built up during the interseismic period. According to their Coulomb stress analysis induced by the 24 January 2020 Elazığ earthquake, a stress load around 1.0 bar was in the north and south parts of the mainshock, in the south-western and north-eastern ends of the aftershock area. (see their Fig. 4). As shown in Fig. 8 in the present study, the smallest *b*-values indicating high positive stress changes and the largest Ma_{max} values were generally observed in the same regions including PtS, ErS and their surroundings. Also, the highest *b*-values are generally related to the other parts of the aftershock area, which have low stress distributions.

Pousse-Beltran *et al*. (2020) aimed to characterize the Elazığ mainshock faulting, its early aftershock activity and postseismic deformation. For this purpose, they used InSAR and optical satellite imagery, teleseismic backprojections, regional moment tensors, and calibrated hypocentral relocations. According to their results, coseismic InSAR modeling provides that only ~20% of the peak slip at depth reaches the surficial model fault patches, suggesting a shallow slip deficit of ~80% and these characteristics probably reflect the low-to-moderate structural maturity of the central EAFZ. Hence, they suggested that the 24 January 2020 earthquake was not characteristic and larger ruptures may be possible. Sayın *et al*. (2021) made a study revealing brief and mechanism-focused technical data of the 24 January 2020 Elazığ-Sivrice earthquake. They also summarized the past and present earthquake characteristics of the region. Beside the geotechnical observations, the general properties of the mainshock and aftershocks and the structural damage due to the earthquake were observed. Moreover, due to liquefaction, soil deformations and lateral spreads were observed. As a result of these deformations, rock falls were seen after the mainshock and aftershocks. For this reason, the regions with the lowest *b*-values, the highest *p*-values and the largest Ma_{max} values may be important in terms of the next earthquake potential in the aftershock area.

Lin *et al*. (2021) investigated the rupture process of the 24 January 2020 Elazığ earthquake by using the teleseismic broadband body-wave and surface-wave records. Also, based on the slip model, they calculated the Coulomb stress changes on the surrounding faults caused by the mainshock. Their results show that the rupture spreads mainly to the south and the mainshock caused stress accumulation to the northern and southern ends of the Elazig-Matalya segment (see their Fig. 9). Thus, this may reactivate the locked fault segment and cause a high seismic hazard in these regions. As seen in Fig. 8 in this paper, the lowest *b*-values indicating high stress changes were observed in the northern and southern parts of the mainshock. Therefore, these regions need a special interest for the future earthquake potential in the study area.

Bayrak, Özer (2021) made a statistical evaluation on the aftershock properties of the 24 January 2020 Sivrice (Elazığ) earthquake by using the *b*-value of the Gutenberg-Richter law, the *p*-value of the modified Omori law and Coulomb stress changes. They calculated the *b*-value as 0.77 and *p*-value as 0.9. Their regional analyses show that *b*-value varies from 0.5 to 1.2, and *p*-value changes between 0.6 and 1.3. They stated that a smaller *b*-value, *p*-value and positive Coulomb values indicate that there is still large stress accumulation in the northeast and southwest parts of the fault. Thus, the findings in the present study are very similar to those of Bayrak, Özer (2021). Hence, these values are correlated with each other and can be used in seismic hazard analysis together.

Alkan *et al*. (2021) carried out a study to investigate the Coulomb stress changes before and after the 24 January 2020 Sivrice (Elazığ) mainshock. Their results show that the stress continued in the northeast and southwest directions from the mainshock and caused a positive Coulomb stress change. They stated that the stress in the study area is at a critical level and these regions can be defined as the earthquake hazard potential area. Therefore, special interest must be given to these anomaly regions such as the north and south directions from the mainshock epicentre (including Gülmahmut, Akçakiraz, Sivrice, Ulutaş, Çevrimtaş, Kavakköy, and Aladikme) and in the south-western end of the region (including Erkenek segment, Pütürge, Uzuntaş, Başmezra, and Pelitli). Consequently, the results of the present study are supported by the findings of Alkan *et al*. (2021).

As discussed in the studies related to the 24 January 2020 Elazığ-Sivrice earthquake, the results obtained in this paper regarding *b*-value, *p*-value, Ma_{max} value, stress distribution and coseismic deformation are supported by the general results provided by Wiemer, Katsumata (1999), Enescu, Ito (2002), Bayrak, Öztürk (2004), Öztürk *et al*. (2008) and Öztürk, Şahin (2019). Also, considering the literature studies on the 24 January 2020 Elazığ-Sivrice earthquake, all results are compatible with each other and this work. Therefore, a comprehensive region-time-magnitude analysis of characteristic aftershock parameters is highly related to aftershock hazard following the mainshock, and these types of evaluations are strongly recommended for a preliminary evaluation after the mainshock.

CONCLUSIONS

A statistical assessment of the characteristic aftershock parameters following the 24 January 2020 M_W = 6.8 Elazığ-Sivrice (Türkiye) earthquake was performed by considering the *b*-value of the Gutenberg-Richter relation, the *p*-value of the modified Omori model, the *Dc*-value of the fractal dimension, and the expected Ma_{max} value for the aftershock occurrence. A small *b*-value (0.82 ± 0.02) for the aftershock sequence may be due to the abundance of aftershocks with $M_L \geq 4.0$. A small *p*-value (0.80 ± 0.02) indicates a slow decay rate of aftershock activity. A large *Dc*-value (1.87 ± 0.07) means that aftershocks are homogeneously distributed and more clustered in smaller areas. The *b*-value changes with time may indicate an increasing trend in the effective stress before the occurrence of larger aftershocks. There exists a clear relation between the regions with the smallest *b*-values and the largest Ma_{max} values. Also, the lowest *b*-value areas are related to high stress regions as well as coseismic deformation regions. The highest *p*-values were observed in the regions associated with the coseismic deformations areas. These results suggest that the variations in *b*-value and *p*-value are highly affected by stress distributions and coseismic deformation following the mainshock. Hence, considering the aftershock hazard following the mainshock, evaluation of the characteristic region-time-magnitude parameters of the aftershock sequences may supply preliminary, reliable and useful results for the fast evaluations of real-time aftershock hazard.

ACKNOWLEDGEMENTS

The author would like to thank the Editor and anonyms reviewers for their useful and constructive recommendations in improving this paper. I thank KOERI for providing free earthquake database via internet. Figures 1b and 1c were plotted using GMT (Generic Mapping Tools) software which is written by Wessel and Smith (1998). The author also thanks Prof. Dr. Stefan Wiemer for providing ZMAP software.

REFERENCES

Adhikari, L.B., Gautam, U.P., Koirala, B.P., Bhattarai, M., Kandel, T., Gupta, R.M., Timsina, C., Maharjan, N., Maharjan, K., Dahal, T., Hoste-Colomer, R., Cano, Y., Dandine, M., Guilhem, A., Merrer, S., Roudil, P., Bollinger, L. 2015. The aftershock sequence of the 2015 April 25 Gorkha-Nepal earthquake. *Geophysical Journal International 203*, 2119–2124. https://doi.org/10.1093/gji/ggv412

Aki, K. 1965. Maximum likelihood estimate of b in the formula log$N = a - bM$ and its confidence limits. *Bulletin of the Earthquake Research Institute*, *Tokyo University 43*, 237–239.

Alkan, H., Büyüksaraç, A., Bektaş, Ö, Işık, E. 2021. Coulomb stress change before and after 24.01.2020 Sivrice (Elazığ) Earthquake (Mw = 6.8) on the East Anatolian Fault Zone. *Arabian Journal of Geosciences 14*, 2648. https://doi.org/10.1007/s12517-021-09080-1

Båth, M. 1965. Lateral inhomogeneities of the upper mantle. *Tectonophysics 2 (6),* 483–514. https://doi.org/10.1016/0040-1951(65)90003-X

Bayrak, Y., Öztürk, S. 2004. Spatial and temporal variations of the aftershock sequences of the 1999 İzmit and Düzce earthquakes. *Earth Planets Space 56*, 933–944. https://doi.org/10.1186/BF03351791

Bayrak, E., Özer, Ç. 2021. The 24 January 2020 (Mw 6.8) Sivrice (Elazig, Turkey) earthquake: a first look at spatiotemporal distribution and triggering of aftershocks. *Arabian Journal of Geosciences 14*, 2445. https://doi.org/10.1007/s12517-021-08756-y

Bender, B. 1983. Maximum likelihood estimation of *b*-values from magnitude grouped data. *Bulletin Seismological Society of America 73*, 831–851.

Bozkurt, E. 2001. Neotectonics of Turkey-a synthesis. *Geodinamica Acta 14*, 3–30. https://doi.org/10.1080/09853111.2001.11432432

Chan, C.H., Wu, Y.M. 2013. Maximum magnitudes in aftershock sequences in Taiwan. *Journal of Asian Earth Sciences 73*, 409–418. http://dx.doi.org/10.1016/j.jseaes.2013.05.006

Cheloni, D., Akinci, A. 2020. Source modelling and strong ground motion simulations for the 24 January 2020, M_w 6.8 Elazığ earthquake, Turkey. *Geophysical Journal International 223* (*2*), 1054–1068. https://doi.org/10.1093/gji/ggaa350

Chen, K., Zhang, Z., Liang, C., Xue, C., Liu, P. 2020. Kinematics and dynamics of the 24 January 2020 *Mw* 6.7 Elazig, Turkey earthquake. *Earth and Space Science 7*, e2020EA001452. https://doi.org/10.1029/2020EA001452

Dieterich, J.H. 1994. A constitutive law for rate of earthquake production and its application to earthquake clustering. *Journal of Geophysical Research 99*, 2601–2618. https://doi.org/10.1029/93JB02581

Duman, T.Y., Emre, Ö. 2013. The East Anatolian Fault: geometry, segmentation and jog characteristics. *Geological Society, London, Special Publications 372*, 495–529. https://doi.org/10.1144/SP372.14

Emre, Ö., Duman, T.Y., Özalp, S., Şaroğlu, F., Olgun, Ş., Elmacı, H., Çan, T. 2018. Active fault database of Turkey. *Bulletin of Earthquake Engineering 16*, 3229–3275. https://doi.org/10.1007/s10518-016-0041-2

Enescu, B., Ito, K. 2002. Spatial analysis of the frequency-magnitude distribution and decay rate of aftershock activity of the 2000 Western Tottori earthquake. *Earth Planets Space 54*, 847–859. https://doi.org/10.1186/BF03352077

Frohlich, C., Willemann, R. 1987. Statistical methods for

comparing directions to the orientations of focal mechanisms and Wadati-Beni of zones. *Bulletin Seismological Society of America 77* (*6*), 2135–2142.

Frohlich, C., Davis, S. 1993. Teleseismic b-values: Or, much ado about 1.0. *Journal of Geophysical Research 98* (*B1*), 631–644. https://doi.org/10.1029/92JB01891

Grassberger, P., Procaccia, I. 1983. Measuring the strangeness of strange attractors. *Physics D9*, 189–208. https://doi.org/10.1016/0167-2789(83)90298-1

Gutenberg, B., Richter, C.F. 1944. Frequency of earthquakes in California. *Bulletin Seismological Society of America 34*, 185–188.

Hainzl, S., Moradpour, J., Davidsen, J. 2014. Static stress triggering explains the empirical aftershock distance decay. *Geophysical Research Letters 41*, 8818–8824. https://doi.org/10.1002/2014GL061975

Helmstetter, A., Shaw, B. 2006. Relation between stress heterogeneity and aftershock rate in the rate-and-state model. *Journal of Geophysical Research 111*, B07304. http://dx.doi.org/10.1029/2005JB004077

Helmstetter, A., Kagan, Y., Jackson, D. 2005. Importance of small earthquakes for stress transfers and earthquake triggering. *Journal of Geophysical Research 110*, B05S08. https://doi.org/10.1029/2004JB003286

Hirata, T. 1989. Fractal dimension of fault systems in Japan: Fractal structure in rock fracture geometry at various scales. *Pure and Applied Geophysics 131* (*1–2*), 157–170.

Kayal, J.R., Das, V., Ghosh, U. 2012. An appraisal of the 2001 Bhuj earthquake (Mw7.7, India) source zone: Fractal dimension and *b* value mapping of the aftershock sequence. *Pure and Applied Geophysics 169*, 2127–2138. https://doi.org/10.1007/s00024-012-0503-7

Kisslinger, C., Jones, L.M. 1991. Properties of aftershock sequences in Southern California. *Journal of Geophysical Research 96* (*B7*), 11947–11958. https://doi.org/10.1029/91JB01200

Lin, X., Hao, J., Wang, D., Chu, R., Zeng, X., Xie, J., Zhang, B., Bai, O. 2020. Coseismic slip distribution of the 24 January 2020 Mw 6.7 Doganyol earthquake and in relation to the foreshock and aftershock activities. *Seismological Research Letters 92* (*1*), 127–139. https://doi.org/10.1785/0220200152

Luginbuhl, M., Rundle, J.B., Turcotte, D.L. 2018. Statistical physics models for aftershocks and induced seismicity. *Philosophical Transactions of the Royal Society A*, *377*, 20170397. https://doi.org/10.1098/rsta.2017.0397

Mandelbrot, B.B. 1982. *The fractal geometry of nature*. San Francisco: Freeman Press.

Marcellini, A. 1997. Physical model of aftershock temporal behaviour. *Tectonophysics 277*, 137–146. https://doi.org/10.1016/S0040-1951(97)00082-6

Mignan, A. 2015. Modelling aftershocks as a stretched exponential relaxation. *Geophysical Research Letters 42*, 9726–9732. https://doi.org/10.1002/2015GL066232

Mogi, K. 1962. Study of the elastic shocks caused by the fracture of heterogeneous materials and its relation to earthquake phenomena. *Bulletin of the Earthquake Research Institute*, *Tokyo University 40*, 125–173.

Nanjo, K.Z. 2020. Were changes in stress state responsible for the 2019 Ridgecrest, California, earthquakes? *Nature Communications 11*, 3082. https://doi.org/10.1038/s41467-020-16867-5

Nanjo, K.Z., Nagahama, H., Satomura, M. 1998. Rates of aftershock decay and the fractal structure of active fault systems. *Tectonophysics 287*, 173–186. https://doi.org/10.1016/S0040-1951(98)80067-X

Nuannin, P., Kulhánek, O., Persson, L. 2012. Spatial and temporal characteristics of aftershocks of the December 26, 2004 and March 28, 2005 earthquakes off NW Sumatra. *Journal of Asian Earth Sciences 46*, 150–160. https://doi.org/10.1016/j.jseaes.2011.12.004

Ogata, Y. 1983. Estimation of parameters in the modified Omori formula for aftershock frequencies by the maximum likelihood procedure. *Journal of Physics of the Earth 31*, 115–124.

Ogata, Y. 2001. Increased probability of large earthquakes near aftershock regions with relative quiescence. *Journal of Geophysical Research 106*, 8729–8744. https://doi.org/10.1029/2000JB900400

Olsson, R. 1999. An Estimation of the maximum *b*-value in the Gutenberg-Richter relation. *Geodynamics 2*, 547–552. https://doi.org/10.1016/S0264-3707(98)00022-2

Omori, F. 1894. On after-shocks of earthquakes. *Journal of the College of Science, Imperial University of Tokyo 7*, 111–120.

Öncel, A.O., Wilson, T.H. 2002. Space-time correlations of seismotectonic parameters and examples from Japan and Turkey preceding the İzmit earthquake. *Bulletin Seismological Society of America 92*, 339–350. https://doi.org/10.1785/0120000844

Öncel, A.O., Main, I., Alptekin, A., Cowie, P. 1996. Spatial variations of the fractal properties of seismicity in the Anatolian fault zones. *Tectonophysics 257*, 189–202. https://doi.org/10.1016/0040-1951(95)00132-8

Özer, Ç., Polat, O. 2017a. Local earthquake tomography of Izmir geothermal area, Aegean region of Turkey. *Bollettino di GeofisicaTeorica ed Applicata 58* (*1*), 17–42. http://doi.org/10.4430/bgta0191

Özer, Ç., Polat, O. 2017b. 3-D crustal velocity structure of Izmir and surroundings. *Journal of the Faculty of Engineering and Architecture of Gazi University 32* (*3*), 733–747. http://doi.org/110.17341/gazimmfd.337620

Öztürk, S. 2009. *An application of the earthquake hazard and aftershock probability evaluation methods to Turkey earthquakes*. PhD Thesis, Karadeniz Technical University, Trabzon, Turkey (in Turkish with English abstract).

Öztürk, S. 2021. Spatio-temporal analysis on the aftershocks of January 24, 2020, Mw6.8 Sivrice-Elazığ (Turkey) earthquake. *International Congress on the Phenomenological Aspects of Civil Engineering, PACE-2021*. Erzurum, Turkey.

Öztürk, S., Şahin, Ş. 2019. A statistical space-time-magnitude analysis on the aftershocks occurrence of the July 21th, 2017 Mw = 6.5 Bodrum-Kos, Turkey, earth-

quake. *Journal of Asian Earth Sciences 172*, 443–457. https://doi.org/10.1016/j.jseaes.2018.10.008

Öztürk, S., Çınar, H., Bayrak, Y., Karslı, H., Daniel, G. 2008. Properties of the aftershock sequences of the 2003 Bingöl, M_D = 6.4, (Turkey) earthquake. *Pure and Applied Geophysics 165*, 349–371. https://doi.org/10.1007/s00024-008-0300-5

Peng, Z., Vidale, J.E., Ishii, M., Helmstetter, A. 2007. Seismicity rate immediately before and after main shock rupture from high-frequency waveforms in Japan. *Journal of Geophysical Research 112*, B03306. http://dx.doi.org/10.1029/2006JB004386

Polat, O., Eyidoğan, H., Haessler, H., Cisternas, A., Philip, H. 2002. Analysis and interpretation of the aftershock sequence of the August 17, 1999, Izmit (Turkey) earthquake. *Journal of Seismology 6*, 287–306. https://doi.org/10.1023/A:1020075106875

Pousse-Beltran, L., Nissen, E., Bergman, E.A., Cambaz, M.D., Gaudreau, É., Karasözen, E., Tan, F. 2020. The 2020 *Mw* 6.8 Elazığ (Turkey) earthquake reveals rupture behaviour of the East Anatolian Fault. *Geophysical Research Letters 47*. e2020GL088136. https://doi.org/10.1029/2020GL088136

Sayın, E., Yön, B., Onat, O., Gör, M., Öncü, M.E., Tunç, E.T., Bakır, D., Karaton, M., Calayır, Y. 2021. 24 January 2020 Sivrice-Elazığ, Turkey earthquake: geotechnical evaluation and performance of structures. *Bulletin of Earthquake Engineering 1* (*9*), 657–684. https://doi.org/10.1007/s10518-020-01018-4

Scholz, C.H. 2015. On the stress dependence of the earthquake *b* value. *Geophysical Research Letters 42*, 1399–1402. https://doi.org/10.1002/2014GL062863

Sedghizadeh, M., Shcherbakov, R. 2022. The Analysis of the aftershock sequences of the recent mainshocks in Alaska. *Applied Sciences 12*, 1809. https://doi.org/10.3390/app12041809

Tajima, F., Kanamori, H. 1985. Global survey of aftershock area expansion patterns. *Physics of the Earth and Planetary Interiors 40*, 77–134. https://doi.org/10.1016/0031-9201(85)90066-4

Tosi, P. 1998. Seismogenic structure behaviour revealed by spatial clustering of seismicity in the Umbria-Marche Region (central Italy). *Annals of Geophysics 41*, 215–224. https://doi.org/10.4401/ag-4331

Tsapanos, T.M., Papazachos, C., Moutafi, Z., Gabrielides, J., Spyrou, T. 1994. Properties of the globally distributed aftershock sequences: Emphasis in the Circum-Pasific Belt. *Bulletin Seismological Society of America XXX* (*5*), 121–158.

Turcotte, D.L. 1992. *Fractals and Chaos in Geology and Geophysics*. New York: Cambridge Univ. Press, 221 pp.

Ulusay, R., Tuncay, E., Sönmez, H., Gökçeoğlu, C. 2004. An attenuation relationship based on Turkish strong motion data and iso-acceleration map of Turkey. *Engineering Geology 74* (*3–4*), 265–291. https://doi.org/10.1016/j.enggeo.2004.04.002

Utsu, T. 1969. Aftershocks and earthquake statistic (I): Some parameters which characterize an aftershock sequence and their interrelation. *Journal of the Faculty of Science, Hokkaido University*, *Series VII* (*2*), 129–195.

Utsu, T. 1971. Aftershock and earthquake statistic (III): Analyses of the distribution of earthquakes in magnitude, time and space with special consideration to clustering characteristics of earthquake occurrence (1). *Journal of the Faculty of Science, Hokkaido University*, *Series VII* (*3*), 379–441.

Utsu, T., Ogata, Y., Matsu'ura, R.S. 1995. The centenary of the Omori formula for decay law of aftershock activity. *Journal of Physics of the Earth 43*, 1–33. https://doi.org/10.4294/jpe1952.43.1

Wang, J.H., Chen, K.C., Leu, P.L., & Chang, C.H. 2016. Studies on aftershocks in Taiwan: A review. *Terrestrial, Atmospheric and Oceanic Sciences 27* (*6*), 769–789. https://doi: 10.3319/TAO.2016.09.12.01

Wei-Jin, X., Jian, W. 2017. Effect of temporal-spatial clustering of aftershocks on the analysis of probabilistic seismic hazard. *Chinese Journal of Geophysics-Chinese Edition 60* (*8*), 3110–3118. https://doi:10.6038/cjg20170818

Wessel, P., Smith, W.H.F. 1998. New, improved version of generic mapping tools released. *EOS Transactions American Geophysical Union 79* (*47*), 579. https://doi.org/10.1029/98EO00426

Westeway, R. 1994. Present-day kinematics of the Middle East and eastern Mediterranean. *Journal of Geophysical Research 99* (*B6*), 12071–12090. https://doi.org/10.1029/94JB00335

Wiemer, S. 2001. A software package to analyze seismicity: ZMAP. *Seismological Research Letters72* (*3*), 373–382. https://doi.org/10.1785/gssrl.72.3.373

Wiemer, S., Wyss, M. 1997. Mapping the frequency-magnitude distribution in asperities: An improved technique to calculate recurrence times. *Journal of Geophysical Research 102*, 15115–15128. https://doi.org/10.1029/97JB00726

Wiemer, S., Katsumata, K. 1999. Spatial variability of seismicity parameters in aftershock zones. *Journal of Geophysical Research 104* (*B6*), 13135–13151. https://doi.org/10.1029/1999JB900032

Wiemer, S., Wyss, M. 2000. Minimum magnitude of completeness in earthquake catalogs: Examples from Alaska, the Western United States, and Japan. *Bulletin Seismological Society of America 90* (*3*), 859–869. http://dx.doi.org/10.1785/0119990114